bioRxiv preprint doi: https://doi.org/10.1101/2020.06.17.157461; this version posted June 18, 2020. The copyright holder for this preprint (which was not certified by peer review) is the author/funder, who has granted bioRxiv a license to display the preprint in perpetuity. It is made available under aCC-BY-NC-ND 4.0 International license.

Wild emmer introgressions alter root-to-shoot growth dynamics under water stress

Harel Bacher[1,2], Feiyu Zhu[3], Tian Gao[3], Kan Liu[5], Balpreet K Dhatt[2], Tala Awada[4], Chi Zhang[5], Assaf Distelfeld[6], Hongfeng Yu[3], Zvi Peleg[1*], Harkamal Walia[2*]

[1.]The Robert H. Smith Institute of Plant Sciences and Genetics in Agriculture, The Hebrew University of Jerusalem, Rehovot, Israel.
[2.]Department of Agronomy and Horticulture, University of Nebraska-Lincoln, Lincoln, NE, USA.
[3.]Department of Computer Science and Engineering, University of Nebraska-Lincoln, Lincoln, NE, USA.
[4.]School of Natural Resources, University of Nebraska-Lincoln, Lincoln, NE, USA.
[5.]School of Biological Sciences, University of Nebraska-Lincoln, Lincoln, NE, USA.
[6.]The Institute of Evolution, University of Haifa, Haifa, Israel.

List of author contributions:

HB, HW, TA and ZP designed the experiments. ZP and AD generated the genetic materials. HB and BD conducted the physiological and transcriptome experiments. FZ, TG and HY processed the image data. HB, KL and CZ performed transcriptome data analysis. HB, HW and ZP wrote the paper. All authors have read and approve the manuscript.

*Corresponding authors: Harkamal Walia, hwalia2@unl.edu and Zvi Peleg, zvi.peleg@mail.huji.ac.il

bioRxiv preprint doi: https://doi.org/10.1101/2020.06.17.157461; this version posted June 18, 2020. The copyright holder for this preprint (which was not certified by peer review) is the author/funder, who has granted bioRxiv a license to display the preprint in perpetuity. It is made available under aCC-BY-NC-ND 4.0 International license.

Abstract

Sustaining wheat (*Triticum* sp.) production during the predicted climatic variability is a major issue for global food security. Wild emmer wheat (*T. turgidum* ssp. *dicoccoides*), the direct progenitor of domesticated wheats is native to semi-arid environments and may offer a novel source of allelic repertoire for enhancing water stress adaptation dynamics. We explored this idea by examining the phenotypic consequence of a series of wild emmer (*acc*. Zavitan) chromatin introgressions into an elite durum wheat (*cv*. Svevo) on water stress adaptation. Wild emmer chromatin introduced divergent water stress responsiveness strategies into wheat, ranging from high plasticity to high stability for biomass accumulation that was concomitant with altered photosynthetic assimilation and water-use efficiency under water-stress conditions. We further characterize promising introgression line (IL20-2), which exhibits high plasticity during water stress. Combination of genotypic information and root transcriptome analysis highlight candidate genes that may regulate this shift in root-to-shoot biomass ratio in response to water stress. We show that introducing alien chromatin in IL20-2 is an instance for enhancing stress adaptation mechanisms that may have been lost during wheat evolution under domestication or breeding.

bioRxiv preprint doi: https://doi.org/10.1101/2020.06.17.157461; this version posted June 18, 2020. The copyright holder for this preprint (which was not certified by peer review) is the author/funder, who has granted bioRxiv a license to display the preprint in perpetuity. It is made available under aCC-BY-NC-ND 4.0 International license.

INTRODUCTION

Wheat (*Triticum aestivum*) is the most widely food crop in the world, providing about 20% of the total dietary calories for human diet (Brouns et al., 2019). To meet the global food demand of the rising population, it is estimated that at least 60% increase in the wheat production is needed by 2050 (Myers et al., 2017). This yield increase needs to be accomplished even as agricultural land is lost to urbanization, industrialization, desertification and climate change that resulting in increased frequency of extreme temperature and precipitation events (Rojas et al., 2019). In the past century, wheat grain yields increment has been largely associated with improved agronomic practices, and genetic enhancements. Developing wheat cultivars with increased biomass accumulation and enhance water-use efficiency under water stress, is one of the core challenges in achieving sustainable global food security. Thus, identification of novel water stress adaptations and their underline mechanisms, will serve as promising genetic resources for breeding.

Plants evolved a suite of adaptive responses to cope with water stress at the molecular, cellular, anatomical, morphological and whole-plant physiological levels (Gupta et al., 2020). These responses can be categorized into three broad types: escape, dehydration avoidance and tolerance. Escape relies on successful completion of reproduction cycle before the onset water stress, achieved by early flowering and/or short growth duration (i.e., developmental plasticity; Kooyers, 2015). Dehydration avoidance is defined as a plant's ability to maintain water potential above a critical threshold in response to water stress (Blum, 1988). This strategy depends on minimizing water loss by reducing transpiration and thus enhancing water-use efficiency. This approach can be achieved by decreasing leaf area and increasing root-to-shoot ratio, or a combination thereof (Araus et al., 2002). Dehydration tolerance is the ability of plants to maintain metabolic activity under low water potential. This is typically coordinated via physiological and biochemical alterations (e.g., osmoregulation) at the cellular and molecular levels (Robbins and Dinneny, 2015), that can be considered as phenotypic plasticity. The ability of an individual to alter its form or function in response to environmental cues, i.e., phenotypic plasticity, plays a key role in adaptation to varying environments (Bradshaw, 1965). Phenotypic plasticity is associated with the developmental rhythm (e.g., germination, plant architecture and size, flowering and maturation timing) and highly affecting plants relative fitness. Plasticity in root system architecture, a tissue that senses water stress early, can contribute to maintenance of water potential for a longer duration by shifting more resources to the roots.

The temporal aspect of plant responses to stress is especially pertinent for water stress responses, as it involves a concomitant change in soil water status along with the physiological

bioRxiv preprint doi: https://doi.org/10.1101/2020.06.17.157461; this version posted June 18, 2020. The copyright holder for this preprint (which was not certified by peer review) is the author/funder, who has granted bioRxiv a license to display the preprint in perpetuity. It is made available under aCC-BY-NC-ND 4.0 International license.

and molecular responses of the plant. Elucidating the underlying genetic basis of phenotypic plasticity requires temporal and spatial measurement of large number of accessions, making this intractable through manual, destructive measurements. With recent advancements in high-throughput, image-based phenotyping platforms, it is becoming more feasible to combine high temporal and spatial resolution phenotyping for linking adaptive responses to underlying allelic variation across populations (Yang et al., 2020). Our ability to identify novel phenotypic responses, for instance under water-limiting environment is not only dependent on technologies to detect these plastic responses but also on the level of phenotypic variation present within the population being examined. The range of phenotypic variation within a background or population can be enhanced significantly by incorporating chromatin from wild or related species as introgression and translocation lines, such as in tomato (*Solanum lycopersicum*; Arms et al., 2015), barley (*Hordeum vulgare*; Baum et al., 2003) and rice (*Oryza sativa*; Tsujimura et al., 2019).

Wild emmer wheat [*T. turgidum* ssp. *dicoccoides* (Körn.) Thell.] is the direct allotetraploid (2n = 4x = 28; genome BBAA) progenitor of all domesticated wheats. Wild emmer thrives across the Near Eastern Fertile Crescent in a wide eco-geographic amplitude and harbors a rich allelic repertoire for numerous agronomic traits, including drought tolerance (Peleg et al., 2005). Introgression of wild emmer alleles has been shown to impact wheat adaptation to water stress, by modification of various traits such as root architecture (Golan et al. 2018; Merchuk-Ovnat et al., 2017), and flower fertility (Golan et al., 2019). Here, we used a new set of wild emmer introgression lines (ILs) in an elite tetraploid wheat background to discover novel phenotypic responses to water stress, with emphasis on the temporal scale by capturing the plant longitudinal nature dynamics. We identified a subset of lines with distinct water stress responses and characterized representative ILs for physiological responses. Molecular analysis of one of the ILs exhibiting a change in root-shoot ratio in response to water-stress yielded candidate genes localizing to the introgression of wild emmer chromatin. Overall, this study shade new light on the potential of wild introgressions to promote various water stress responsiveness dynamics, as well as characterization of water stress adaptive mechanism that can serve as basis for future climate resilience wheat breeding programs.

bioRxiv preprint doi: https://doi.org/10.1101/2020.06.17.157461; this version posted June 18, 2020. The copyright holder for this preprint (which was not certified by peer review) is the author/funder, who has granted bioRxiv a license to display the preprint in perpetuity. It is made available under aCC-BY-NC-ND 4.0 International license.

RESULTS

Wild emmer introgressions confer divergent water stress responses

We hypothesized that introducing a series of wild emmer introgressions in an elite durum wheat cultivar could increase the range of phenotypic responses to water stress, without significantly compromising its desirable agronomic traits. The assumption being that introgression of small wild emmer genomic portion is sufficient to alter the domesticated wheat water stress response. To address this question, we selected a subset of 47 wild emmer introgression lines (ILs) in the background of elite durum wheat *cv*. Svevo, consists 1.3-14.2% of Zavitan genes per IL (Supplemental Table S1), to examine for their phenotypic responses to water stress. We applied a non-destructive, image-based phenotyping approach to compare the temporal shoot growth under well-watered (WW; 80% field capacity) and water-limited (WL; 30% field capacity) treatments. Five side view images were used to obtaining the pixel counts as an estimate for daily shoot biomass accumulation as described before (Knecht et al., 2016). In general, the growth curves for Svevo were similar to the median response of all ILs collectively during the course of the experiment, suggesting that ILs biomass accumulation (projected shoot area, PSA) were segregating around Svevo performance (Fig. 1A). Notably, most of the ILs reached the target of 30% field capacity after 19 days (ranging from 14 to 24 days) whereas significant differences in biomass accumulation was detected already after 10 days (collectively), which indicate the wide strategies of responses to water stress.

bioRxiv preprint doi: https://doi.org/10.1101/2020.06.17.157461; this version posted June 18, 2020. The copyright holder for this preprint (which was not certified by peer review) is the author/funder, who has granted bioRxiv a license to display the preprint in perpetuity. It is made available under aCC-BY-NC-ND 4.0 International license.

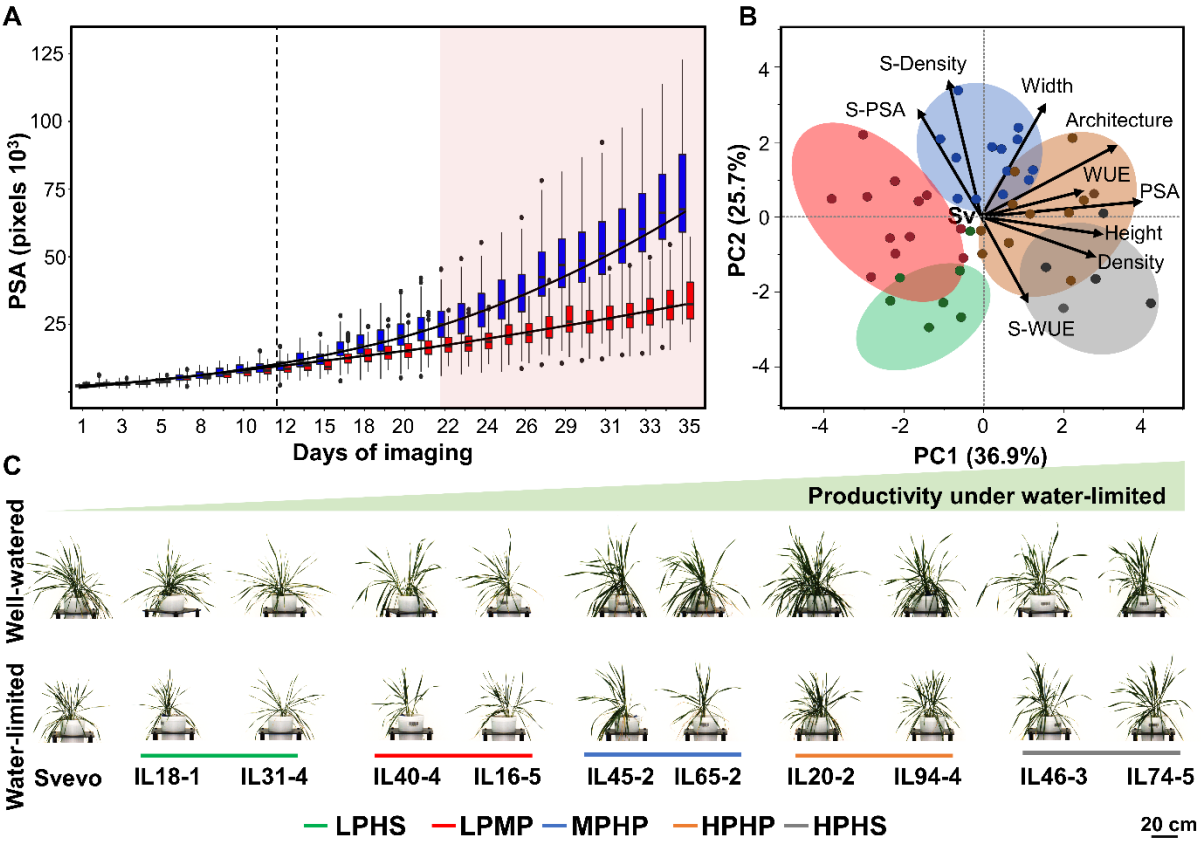

Figure 1. Wild introgressions promote phenotypic diversity. (A) Longitudinal dynamics of biomass accumulation (projected shoot area; PSA) for the 47 introgression lines collectively. The parental line Svevo marked with black solid line. (B) Principal component (PC) analysis of continuance morpho-physiological traits under WL conditions and expressed as drought susceptibility index (S). Biplot vectors are trait factor loadings for PC1 and PC2. Water-use efficiency (WUE), biomass accumulation (PSA), plant architecture, density, height and width, and in term of drought susceptibility index for WUE (S-WUE), biomass accumulation (S-PSA) and density (S-density). The five clusters of stress responsiveness: high productivity - high stability (HPHS; gray), high productivity - high plasticity (HPHP; Orange), moderate productivity-high plasticity (MPHP; Blue), low productivity-moderate plasticity (LPMP; Red), low productivity-high stability (LPHS; Green). (C) Representative photo of ILs from each responsiveness cluster under contrasting water availabilities, after 35 days of imaging.

Next, we extracted some of the key morphological traits derived from RGB images included, PSA, plant height and width, plant architecture (convex area), and plant density, and divided PSA with total water-use to obtain water-use efficiency (WUE) at the final day of the experiment. In order to determine the extent of phenotypic diversity for the morphological traits introduced in the Svevo background, we plotted the density distribution of the ILs under WW and WL treatments at the 35 d time point. The ILs exhibit a broad range for all the traits with Svevo positioned close to the average value for most traits (Supplemental Fig. S1). This result suggests that introgression of small pieces of chromatin from wild emmer into a wheat background can introduce significant phenotypic diversity. While ILs panel showed strong reduction in PSA, as indicated by the separation between WL and WW, and in 50% reduction of Svevo. Greater phenotypic overlap between WW and WL was observed in plant width,

bioRxiv preprint doi: https://doi.org/10.1101/2020.06.17.157461; this version posted June 18, 2020. The copyright holder for this preprint (which was not certified by peer review) is the author/funder, who has granted bioRxiv a license to display the preprint in perpetuity. It is made available under aCC-BY-NC-ND 4.0 International license.

density and WUE. The phenotypic distribution for plant height among the ILs under WL treatment was wider as compared with WW treatment. Notably, the phenotypic range for WUE is much broader under WL compared to the WW conditions.

To better understand the relationships among the morpho-physiological traits, we performed correlation analysis between these traits at 35 d (Supplemental Fig. S2 and Supplemental Table S2). PSA was positively correlated with all morphological traits suggesting that plant biomass and architecture are tightly associated regardless of water availability. Under WL, PSA and plant density were found positively correlated with WUE, suggesting that plant architecture can affect the WUE under stress. To further explore the water stress response of these phenotypic traits, we performed principal component analysis (PCA) of the morpho-physiological traits under WL treatment as well as in relative terms (i.e., S index) (Fig. 1B). PCA extracted three major PCs (Eigen values > 1.2) accounting collectively for 76% of the phenotypic variance among the ILs (Supplemental Fig. S3). PC1 explained 36.9% of the dataset variation and loaded positively with PSA, plant height, plant architecture, WUE and plant density. PC2 explained 25.7% of the dataset variation and loaded positively with plant width, S-PSA and S-density and negatively with S-WUE. PC3 explained 13.4% of the dataset variation and loaded positively with WUE, S-PSA and plant density. To further dissect the differences in ILs water stress responsiveness, we performed hierarchical clustering analysis of the morpho-physiological traits under WL treatment and derived stress index traits (Supplemental Fig. S4). The clustering analysis resolved the ILs into five distinct clusters, which could broadly be described as following: Cluster 1 (high productivity and high stability, HPHS), Cluster 2 (high productivity and high plasticity, HPHP), Cluster 3 (moderate productivity and high plasticity, MPHP), Cluster 4 (low productivity and moderate plasticity, LPMP), and Cluster 5 (low productivity and high stability, LPHS). The productivity in context of this study implies biomass accumulation under WL.

Based on this analysis, Svevo resolved to Cluster 4 (LPMP) that characterized as low PSA and WUE, with intermediate response to water stress. The two most productive clusters (HP), Cluster 1 and Cluster 2 showed different stress response as expressed in the drought susceptibility index. Cluster 1 exhibited low S-PSA values which indicate lower change between WW and WL treatments. Cluster 2 showed the highest WUE under WL and relatively high values of S-PSA, resulting with a high plasticity cluster. Overall, raw images of representative plants from the five responsiveness clusters under both water treatments can demonstrate the different stress responsiveness clusters (Fig. 1C).

bioRxiv preprint doi: https://doi.org/10.1101/2020.06.17.157461; this version posted June 18, 2020. The copyright holder for this preprint (which was not certified by peer review) is the author/funder, who has granted bioRxiv a license to display the preprint in perpetuity. It is made available under aCC-BY-NC-ND 4.0 International license.

Water stress responsiveness classification based on temporal growth dynamics

Although the clustering analysis using endpoint measurements of the ILs provide a useful perspective, the temporal dynamics for these traits that precede these phenotypic outcomes can elucidate the responsiveness to water stress. To address this, we mapped the overall trajectories and phenotypic distributions of these traits on a weekly scale (Fig. 2A). In general, all clusters exhibited higher biomass accumulation and higher coefficient of variance (CV) under WW as compared with WL treatment (Supplemental Table S3). The PSA distributions under WW and WL treatments show that the high stability (HS) clusters exhibited substantial overlap between the WW and WL curves in weeks 5 and 6. The point of significant response to water stress, determined as three continuous days of significant ($P \leq 0.05$) difference in growth between treatments, ranged between 10 days (HPHP cluster) to 26 days (HPHS cluster) (Fig. 2A; Supplemental Table S4). A similar pattern was found for plant architecture and density (Supplemental Fig. S5). The parental line (Svevo; LPMP cluster) expressed an intermediate response (17, 18 and 15 days for PSA, plant architecture and density, respectively; Supplemental Fig. S5). Although, MPHP cluster exhibits high biomass accumulation under WW treatment, it was labeled as moderate productivity (MP) based on its performance under WL treatment. The clusters classification to productivity (i.e., HP, MP and LP) were found significantly different from each other ($P<10^{-4}$) under WL.

Plant responsiveness clusters expressed in heritability dynamics

To dissect the genetic (G) and environmental (E) components of PSA, underlying each responsiveness cluster through developmental stages, we calculated broad-sense heritability and its components. The HPHS cluster exhibited the highest genetic component (sigma^2 G), which increased with progression of water stress duration (Fig. 2B). On the other hand, HPHP and MPHP clusters, had lower genetic components and the highest G×E interaction (Sigma^2 G×E) (Fig. 2B, C). The broad-sense heritability dynamics ($_{bs}h^2$) of PSA showed clear separation into stability (LPHS and HPHS) and plasticity (LPMP, MPHP, and HPHP) (Fig. 2D). In general, the level of PSA $_{bs}h^2$ decreased over time. Heritability dynamics of plant density showed a strong genetic component for HPHP and a high environmental effect for LPMP that increased over time. Plant architecture presented a high environmental effect on MPHP, causing low $_{bs}h^2$ for this cluster (Supplemental Fig. S6). Overall, the heritability dynamics of the responsiveness cluster emphasis that stability and plasticity derived from both genetic and environmental effect that can be phenotype and genetically controlled.

bioRxiv preprint doi: https://doi.org/10.1101/2020.06.17.157461; this version posted June 18, 2020. The copyright holder for this preprint (which was not certified by peer review) is the author/funder, who has granted bioRxiv a license to display the preprint in perpetuity. It is made available under aCC-BY-NC-ND 4.0 International license.

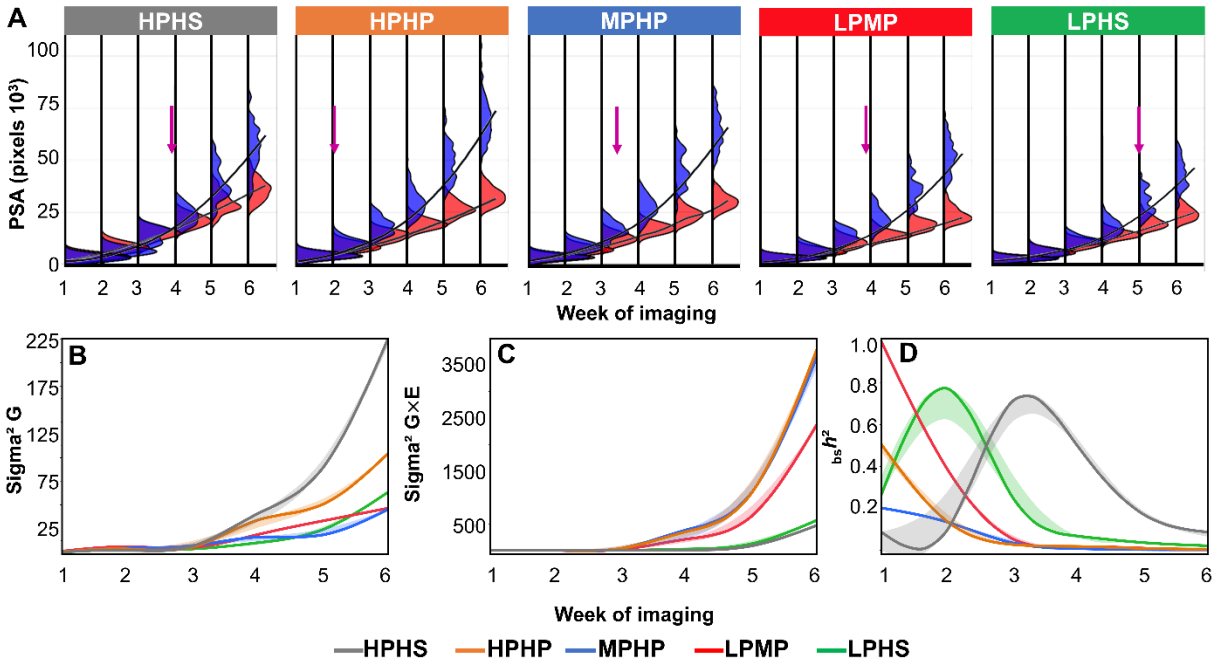

Figure 2. Longitudinal dynamics of the five responsiveness clusters. (**A**) Longitudinal frequency distribution of biomass accumulation (projected shoot area; PSA) of each responsiveness cluster under well-watered (WW; blue) and water-limited (WL; red) treatments. The five clusters of stress responsiveness: high productivity - high stability (HPHS; gray), high productivity - high plasticity (HPHP; Orange), moderate productivity-high plasticity (MPHP; Blue), low productivity-moderate plasticity (LPMP; Red), low productivity-high stability (LPHS; Green). The point of significant ($P \leq 0.05$) response to water stress is marked above with arrow. Longitudinal heritability components of (**B**) genetic (Sigma^2 G), (**C**) environmental interaction (Sigma^{2}G × E), and (**D**) broad sense heritability ($_{bs}h^2$).

IL20-2 exhibited higher assimilation rate under water-limited conditions

Although the ILs were broadly categorized into five distinct clusters, given the focus of this work on phenotypic plasticity in response to water stress, we decided to compare the two high productivity clusters HPHP and HPHS, represented by IL20-2 and IL46-3, respectively, for downstream physiological experimentation and analysis. We targeted the temporal window during the early stages of previous experiment so that we can characterize the initial phase of separation in growth rate and water stress response. Under WL treatment, the relative growth rate dynamics demonstrated the advantage of the two productive clusters (linear equation slope 369.0 and 679.1 for IL20-2 and 46-3, respectively) compared to Svevo (302.5) (Fig. 3A; Supplemental Table S5). While IL46-3 maintained a similar linear equation slope under both water treatments, IL20-2 exhibited a stronger change in regression pattern (854.9 *vs.* 369.0 for WW and WL, respectively; Fig. 3A) confirming its high plasticity in response to water stress. In general, assimilation rate (A) dynamics declined with the progression of water stress. Svevo exhibited the highest reduction (34.9%), whereas the high stability IL46-3 had only 13.1% reduction (Fig. 3B). Notably, IL20-2 exhibited the highest assimilation rate under WW treatment over time (29.68 µmol m^{-2} s^{-1}), whereas under WL both IL46-3 and IL20-2 exhibited

bioRxiv preprint doi: https://doi.org/10.1101/2020.06.17.157461; this version posted June 18, 2020. The copyright holder for this preprint (which was not certified by peer review) is the author/funder, who has granted bioRxiv a license to display the preprint in perpetuity. It is made available under aCC-BY-NC-ND 4.0 International license.

similar A (23.49 and 23.28 µmol m^{-2} s^{-1}, respectively) which was significantly higher than Svevo (P=0.03). In addition, IL20-2 exhibited significantly higher (P=0.046) stomatal conductance (g_s) under WL as compared with Svevo at the last day of measurements (0.33 *vs.* 0.20 mol m^{-2} s^{-1}, respectively; Fig. 3C). Under WW, IL20-2 exhibited the highest transpiration rate (E), whereas all three lines had similar transpiration rates under WL. This pattern fits into IL20-2 HPHP pattern that keeps high biomass accumulation and strong phenotypic response to water stress. (Supplemental Fig.S7; Supplemental Table S6).

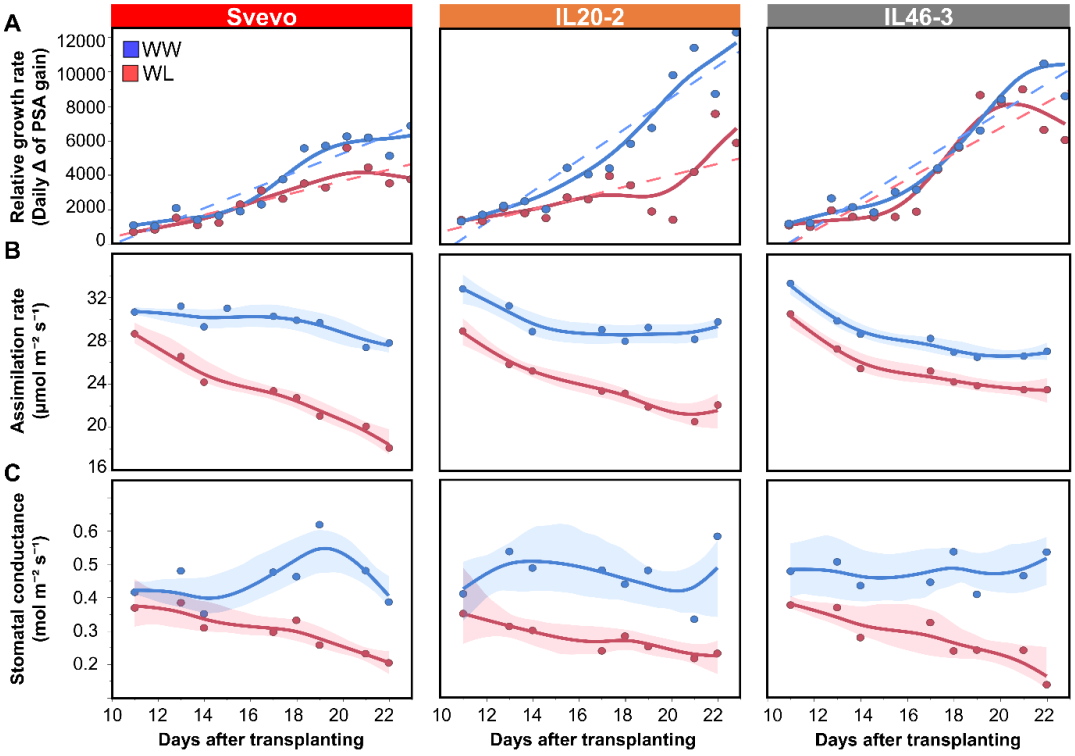

Figure 3. Longitudinal dynamics of Svevo, IL20-2 and IL46-3 for (**A**) relative growth rate, (**B**) net assimilation rate and (**C**) stomatal conductance under well-watered (WW; blue) and water-limited (WL; red) treatments.

IL20-2 exhibits higher root-to-shoot ratio under water stress

To test if better water capture involves in the physiological advantage of IL20-2 higher gas exchange and growth rate under WL, we targeted the root system (Fig. 4A). We measured root dry weights from soil grown 21 d old plants and found that both IL46-3 and IL20-2 had higher root biomass relative to Svevo (P≤0.001) under WW treatment. However, under WL treatment, IL20-2 root biomass increased significantly compared to Svevo (P=0.003). Further, IL20-2 also exhibits higher root-to-shoot ratio when compared with Svevo under WL conditions (P=0.046) (Fig. 4B, C; Supplemental Table S7). This data suggests that IL20-2 does have a root response to water stress that is divergent from Svevo under water stress. To explore this differential root response on a temporal scale, we performed a seedling stage assays using paper roll set-up and collected root samples for RNA sequencing. While the shoot length of IL20-2 and Svevo was

bioRxiv preprint doi: https://doi.org/10.1101/2020.06.17.157461; this version posted June 18, 2020. The copyright holder for this preprint (which was not certified by peer review) is the author/funder, who has granted bioRxiv a license to display the preprint in perpetuity. It is made available under aCC-BY-NC-ND 4.0 International license.

similar under WW and WL treatments, IL20-2 exhibited significantly higher root length throughout the experiment, with 10.3% longer roots at the last day of the experiment (25.21 *vs.* 22.85 cm, for IL20-2 and Svevo, respectively; P=0.006) under WL. This advantage expressed in the higher (12.5%) root-shoot ratio of IL20-2 compared with Svevo at the last day (P=0.001; Supplemental Fig. S8 A-F). This suggested that root growth dynamic of IL20-2 are different from Svevo even during early seedling stage and more apparent under WL treatment with a significant effect of increasing the root-to-shoot ratio. Importantly, our results show that root biomass in later stages and root length at seedling stage showed similar trend of advantage in IL20-2 under WL treatment (Fig. 4, Supplemental Fig. S8).

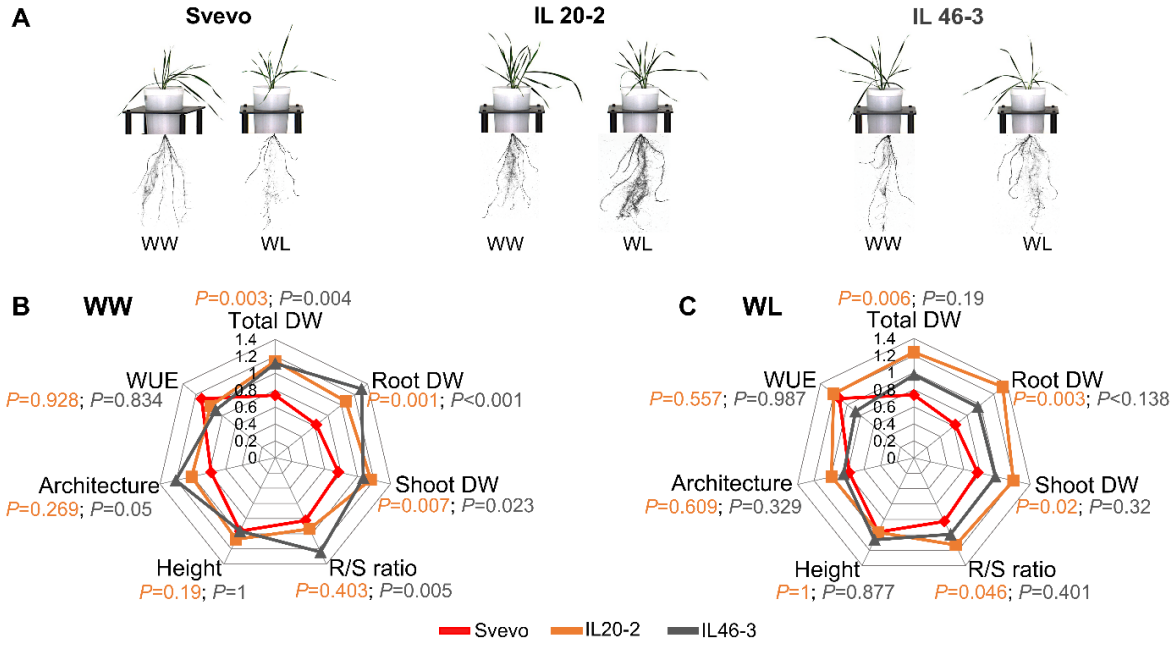

Figure 4. Morpho-physiological modification in response to water stress. (**A**) Representative photo of Svevo, IL20-2 and IL46-3 under well-watered (WW) and water-limited (WL) treatments. Photo taken 14 days after transplanting. Radar charts comparing the phenotypic traits of Svevo (red), IL20-2 (orange) and IL46-3 (gray) plants under (**B**) WW and (**C**) WL treatments. Values are means (n=4). Total dry weight (Total DW), water-use efficiency (WUE), plant architecture (convex area), plant height (Height), root-to-shoot ratio (R/S ratio), shoot DW and root DW.

IL20-2 wild introgressions exhibit higher DEG frequency as expressed in water response

Given the differential root growth and root-to-shoot ratio between Svevo and IL20-2 in the seedling stage, we reasoned that the underlying gene(s) responsible for these phenotypes could be the same that resulted in similar root-to-shoot ratio plasticity observed in later vegetative stages. Therefore, we performed transcriptome analysis on roots from seedling stage experiment with the goal of identifying candidate genes that underlie the root-to-shoot plasticity phenotype. Seedling roots sampling for transcriptome is more precise as it prevents root damage

bioRxiv preprint doi: https://doi.org/10.1101/2020.06.17.157461; this version posted June 18, 2020. The copyright holder for this preprint (which was not certified by peer review) is the author/funder, who has granted bioRxiv a license to display the preprint in perpetuity. It is made available under aCC-BY-NC-ND 4.0 International license.

that occurs with sampling roots from older plants growing in soil or sand. We combined the transcriptomics with high-density genotypic data of IL20-2 and Svevo to map the differentially expressed genes (DEGs) to specific introgressions. IL20-2 has three introgressions from Zavitan, the wild emmer parent, on chromosomes 2A (3.7 Mbp), 4A (23 Mbp) and 5B (6.7 Mbp), accounting for ~0.33% of the tetraploid durum wheat genome (Maccaferri et al., 2019). Based on public annotations, a total of 651 genes (73, 503 and 75, respectively; Avni et al., 2017; Supplemental Table S8) map to these introgressions. Under water-limited, when the root phenotype is most apparent, we identified 599 DEGs (Fig. 5A) between Svevo and IL20-2, with 37 genes (6.17%) co-localizing to the introgressions.

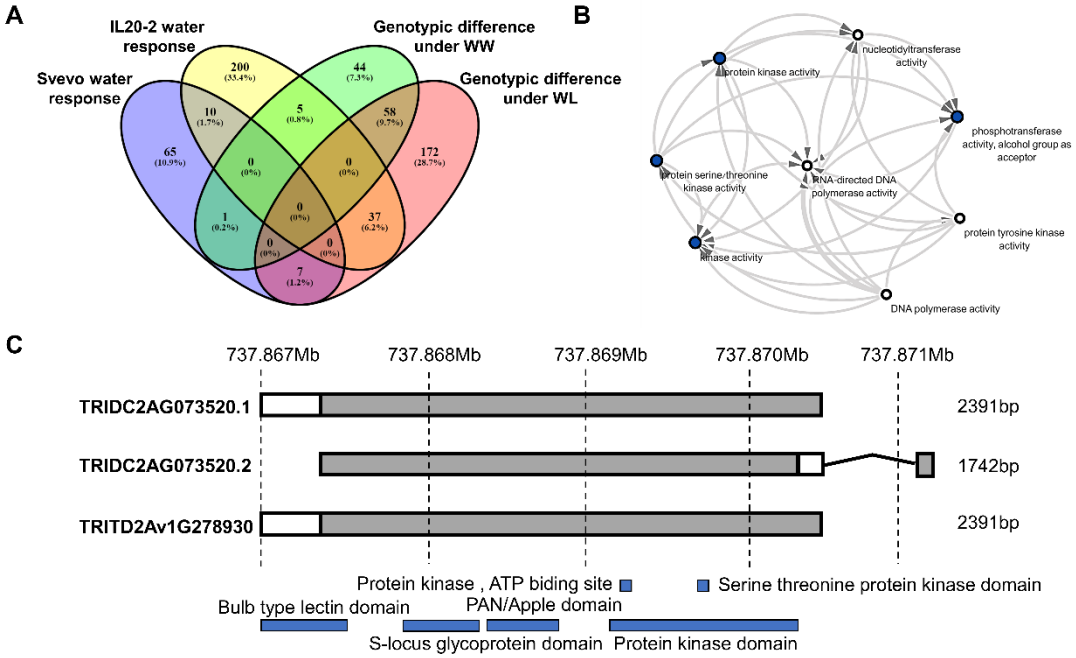

Figure 5. Differently expressed genes (DEGs) dynamics. (**A**) A four-way Venn diagram of DEGs among IL20-2 and Svevo under well-watered (WW) and water-limited (WL) treatments. (**B**) Network expression pattern of the DEGs associated with kinase activity. Node with blue color represent high interaction. (**C**) Splice variation of TRIDC2AG073520 gene.

Of these, 425 genes were down-regulated and 174 genes were up-regulated in IL20-2 (Supplementary Table S9). Under WL treatment, 39.23% of the DEGs were differently expressed between Svevo and IL20-2 (56 up- and 179 down-regulated), whereas only 11.35% were expressed differently under WW treatment. Gene Ontology (GO) analysis revealed three main biological processes: metabolic processes (GO:0008152; $P<10^{-4}$), localization (GO:0051179; $P<10^{-4}$) and response to stimulus (GO:0050896; $P<10^{-4}$) (Supplemental Fig. S9A). The molecular functions were associated with antioxidant activity (GO:0016209; $P<10^{-4}$), catalytic activity (GO:0003824; $P<10^{-4}$), transporter activity (GO:0005215; $P<10^{-4}$) and transferase activity (GO:0016740; $P<10^{-4}$) (Supplemental Fig. S9B).

bioRxiv preprint doi: https://doi.org/10.1101/2020.06.17.157461; this version posted June 18, 2020. The copyright holder for this preprint (which was not certified by peer review) is the author/funder, who has granted bioRxiv a license to display the preprint in perpetuity. It is made available under aCC-BY-NC-ND 4.0 International license.

Candidate genes associated with longer roots under water stress

To examine if the root plasticity trait of IL20-2 could be due to differentially abundant transcript(s) that localize to the introgression, we filtered for these DEGs and identified 17 DEGs under WW and 18 DEGs under WL treatments between IL20-2 and Svevo. Two DEGs (TRIDC4AG049220 and TRIDC4AG049940) were found to express uniquely in IL20-2 in response to water stress. To find the causal genes associated with the IL20-2 root phenotype, we targeted root-related DEGs, which resulted in five candidate genes (CG; Supplementary Table S10). The criteria used to filter for these five genes are based literature searches of orthologs with root associated phenotypes. Three of these genes were up-regulated in IL20-2 under WL (TRIDC4AG046080, TRIDC4AG048600 and TRIDC2AG073520), one gene was down-regulated under WL (TRIDC4AG046660) and one gene (TRIDC4AG046110) showed up-regulation under WW treatment only. Of these five genes, TRIDC4AG046080 is low confidence gene based on annotation of the Zavitan genome. The other four genes carried mutations or did not found in the domesticated allele compared with the wild emmer (Supplementary Table S10).

TRIDC4AG046110 is a *FAR1-RELATED SEQUENCE 4-like* isoform that was shown to be down-regulated in salt-susceptible sweet sorghum (*Sorghum bicolor*) roots (Yang et al., 2018). TRIDC4AG048600 is a *SIMILAR TO RCD ONE 1* (*SRO1*) gene. In *Arabidopsis* (*Arabidopsis thaliana*), a double mutant of *AtSRO1* exhibited shorter roots and a smaller cell division zone as compared with wild-type plants (Teotia and Lamb, 2011). A sequence alignment of this gene against the Zavitan genome indicates a truncated protein in the Zavitan genome that may result in loss of function or a modified function.

The remaining three DEGs were associated with protein kinase function (Supplementary Table S10), were network analysis of molecular functions showed significance of downstream transferase activity elements in various kinase activities (Fig. 5B). In details, TRIDC4AG046080 is a homologue of a rice domain of unknown function (*DUF581*) that, in *Arabidopsis*, was found to play a role in sucrose non-fermenting-related kinase (*SnRK1*) (Nietzsche et al., 2016). TRIDC4AG046660 is a Leucine-rich repeat receptor protein kinase (LRR-RLK) and TRIDC2AG073520 is a G-type lectin S-receptor-like serine/threonine-protein kinase (RLK). We examined sequence of TRIDC2AG073520 in the Zavitan genome (Avni et al., 2017) and identified two splice variants on chromosome 2A, which are 2391bp and 1742bp for TRIDC2AG073520.1 and TRIDC2AG073520.2, respectively. In contrast, only a single variant (2391bp) was found in the tetraploid durum wheat (*cv*. Svevo) and hexaploid bread wheat (*cv*. Chinese Spring; Appels et al., 2018) genomes (Fig. 5C). This CG was mapped in

bioRxiv preprint doi: https://doi.org/10.1101/2020.06.17.157461; this version posted June 18, 2020. The copyright holder for this preprint (which was not certified by peer review) is the author/funder, who has granted bioRxiv a license to display the preprint in perpetuity. It is made available under aCC-BY-NC-ND 4.0 International license.

the expression atlas of Zavitan to root tissue- specific gene and enforce our hypothesis of this CG as the main candidate (Supplemental Fig. S10).

DISCUSSION

Wild plants developed various reversible and non-reversible phenotypic plasticity strategies to cope with environmental uncertainty. In contrast, man-made selection under optimal environmental conditions resulted in higher crop-plants phenotypic stability (Reynolds et al., 2007; Placido et al., 2013; Lopes et al., 2015). As a consequence, many of the modern cultivars may not fit for the projected climate change scenarios in many regions (Kissoudis et al., 2016). Wild ancestors of modern crop-plants offer promising source for genetic diversity and novel drought adaptive traits yet to be exploited. Here, we used a set of wild emmer introgression lines to study their dynamic responsiveness to water stress and its underlying genetic mechanisms.

The introgression of Zavitan alleles into modern durum cultivar promoted higher phenotypic diversity under both WW and WL treatments, as expressed in plant architecture and biomass accumulation (Fig. 1). While the IL panel was developed from single wild emmer accession (Zavitan), it resulted in wide segregation of morpho-physiological traits (either positively or negatively). This accession originated from habitat with high soil moisture fluctuations, due to shallow brown basaltic soil type, that have been show to promote diversity (Poot and Lambers, 2008; Peleg et al., 2008). This phenotypic variation is associated with the quantitative nature of these traits and the different combinations of wild and domesticated alleles. Interestingly, the mean biomass accumulation trajectory over time of the IL panel was similar to Svevo under both water treatments.

Water stress reduced about 50% of biomass (i.e., PSA) and altered plant architecture (i.e., convex area 12.5-48.5%) relatively to the WW treatment (Supplementary Fig. S1), with both variables being positively associated with one another (Supplementary Fig. S2). Increased phenotypic variation in response to water stress was quantified by the calculation of drought susceptibility index (S-index). The combination of IL performance under WL with their S-indexes resulted in five distinct clusters of high phenotypic stability (HPHS, LPHS) and phenotypic plasticity (HPHP, MPHP, LPMP). Phenotypic stability is often associated with small changes in plant performance in response to unfavorable conditions. Escape, i.e., rapid growth to avoid the stress, is a common strategy of wild plants in xeric habitats, and has been repeatedly reported for many wild grasses such as wild emmer wheat (Peleg et al., 2005),

bioRxiv preprint doi: https://doi.org/10.1101/2020.06.17.157461; this version posted June 18, 2020. The copyright holder for this preprint (which was not certified by peer review) is the author/funder, who has granted bioRxiv a license to display the preprint in perpetuity. It is made available under aCC-BY-NC-ND 4.0 International license.

Brachypodium distachyon (Opanowicz et al., 2008), and *Avena barbata* (Sherrard and Maherali, 2006). Accordingly, the two clusters exhibiting phenotypic stability had biomass reductions of only 45 and 40% for LPHS and HPHS, respectively. Interestingly, the LPHS had characteristics of "small plants" (PSA, 50.4 and 27.8 kPixel for WW and WL, respectively), whereas HPHS had high biomass under WW and the highest values among all clusters under WL (67.1 and 40.6 kPixel, respectively). These results suggest that phenotypic stability strategy is not size-dependent, but rather an active mechanism that enables plants to cope with water stress.

Wild emmer wheat populations were found to harbor rich phenotypic diversity for drought-adaptive traits, which correspond with the wide inter-annual and seasonal fluctuations in soil moisture availability of the Mediterranean basin (Peleg et al., 2005). Accordingly, the phenotypic plasticity clusters exhibited high reduction in biomass accumulation (55 and 56% for MPHP and HPHP, respectively). The HPHP cluster had the highest biomass under WW (PSA 81.8 kPixel); while under WL it exhibits high reduction, biomass was still relatively high (36.4 kPixel) compare to all clusters.

Plant acclimation to water stress elicited physiological, morphological and metabolic responses that occurred through coordinated spatio-temporal processes. These processes changed the physiological status of plants toward a new steady-state level that supported growth and fitness under unfavorable conditions. Time-course characterization of the responsiveness clusters showed that phenotypic plasticity clusters responded earlier (12, 8 and 10 kPixel for LPMP, MPHP and HPHP, respectively), then stability clusters (20 and 26 kPixel for LPHS and HPHS, respectively) (Fig. 2A). In order to understand the longitudinal genetic architecture of the responsiveness clusters, we calculated broad sense heritability ($_{bs}h^2$) dynamics. While the plasticity clusters exhibited a decrease in PSA $_{bs}h^2$ over time as a consequence of high G×E interaction (Sigma^2 G×E) and low genetic component (Sigma^2 G), the stability clusters showed increased heritability during early growth and decreased heritability at later stages, which corresponds to the late stress responses (Fig. 3).

Plants exhibit morphological and physiological adjustments to maintain water status and carbon assimilation under water stress (Chaves et al., 2009). The two high productivity clusters (i.e., HPHS and HPHP) exhibited contrasting response mechanisms, with the plasticity cluster responding earlier (Δ16, Δ17 and Δ8 days, for PSA, plant density and plant architecture, respectively; Fig. 2; Supplementary Fig. S5). Detailed characterization of these two clusters (represented by IL20-2 and IL46-3 for HPHP and HPHS, respectively) confirmed the earlier response of HPHP in terms of relative growth rate (Fig. 3A), thus suggesting a non-size

bioRxiv preprint doi: https://doi.org/10.1101/2020.06.17.157461; this version posted June 18, 2020. The copyright holder for this preprint (which was not certified by peer review) is the author/funder, who has granted bioRxiv a license to display the preprint in perpetuity. It is made available under aCC-BY-NC-ND 4.0 International license.

dependent plant responsiveness to water stress. In agreement, while IL46-3 maintained similar photosynthetic and transpiration rates under WW and WL, IL20-2 responded as early as day 12, limiting its assimilation rate. Notably, IL20-2 had the highest photosynthetic rate under WW and exhibited the larger reduction under WL; yet, it was still significantly better than Svevo.

A fast stress responsiveness strategy may negatively affect carbon assimilation and growth; on the other hand, early acclimation can trigger a metabolic shift of carbon allocation to different plant organs (Rodrigues et al., 1993; Bohnert and Sheveleva, 1998). Thus, under limited water availability root-to-shoot ratio plasticity can mediate optimal resource partitioning between growth and development (Shipley and Meziane, 2002; Voss-Fels et al., 2018). Modern bread wheat cultivars have lower root-to-shoot ratios as compared with old traditional cultivars (landraces) (Siddique et al., 1990). Moreover, a comparison among wild emmer, domesticated emmer and durum wheat showed a trend of reduced root-to-shoot during the initial domestication from wild to domesticated emmer, and during wheat evolution under domestication (Gioia et al., 2015; Roucou et al., 2018). Accordingly, the introgression of alleles from Zavitan in the background of the elite durum wheat cultivar significantly increased the root-to-shoot ratio (30%) under WL as compared with the parental line (Fig. 4C). Likewise, Merchuk-Ovnat et al. (2017) reported higher root-to shoot ratio in response to water stress from wild emmer (acc. G18-16) introgression in background of elite bread wheat cultivar. Thus, introducing new genetic diversity for root-to-shoot ratio plasticity from wild progenitors will facilitate resilience of modern wheat cultivars to the projected fluctuating water availability during the growing season.

The root system is the site of interactions with the rhizosphere; thus, root architectural plasticity (i.e., allocational, morphological, anatomical, or developmental) is critical adaptation strategy to environmental cues (Rellán-Álvarez et al., 2016; Golan et al., 2018). To better understand the genetic mechanism associated with the increased root biomass of IL20-2, we analyzed transcriptional patterns of roots under water stress. In general, transcriptional modifications of IL20-2 in response to water stress were significantly greater than Svevo (223 *vs*. 73 DEGs, respectively). Likewise miRNA expression in the roots of two wild emmer accessions (TR39477 and TTD-22) were significantly higher compared with domesticated durum wheat (*cv*. Kızıltan) under water stress (Akpinar et al., 2015). These results emphasize the potential of higher plasticity in wild relatives as compared to the domesticated genepool.

Downstream gene network analysis highlighted the key role of protein kinases as hubs of interaction (Fig. 5B). Three CGs (TRIDC4AG046080, TRIDC2AG073520 and

bioRxiv preprint doi: https://doi.org/10.1101/2020.06.17.157461; this version posted June 18, 2020. The copyright holder for this preprint (which was not certified by peer review) is the author/funder, who has granted bioRxiv a license to display the preprint in perpetuity. It is made available under aCC-BY-NC-ND 4.0 International license.

TRIDC4AG046660) were found associated with protein kinase function that mediates plant hormone and nutrient signaling, and cell cycle regulation (Laurie and Halford, 2001; Virlet et al., 2017). TRIDC4AG046660 is a leucine-rich repeat receptor-like protein kinase (LRR-RLK). Mutants of this gene in *Arabidopsis* (*At*2g33170) control root growth and are mediated by cytokinin (Colette et al., 2011). TRIDC4AG046080 (DUF581 in rice) interact with *SnRK1* and regulated by hormones and differentially regulated by hormones and environmental signals (Nietzsche et al., 2016). Wheat mutants containing a conserved DUF581 domain revealed a salt-induced gene (TaSRHP). Over-expression of this gene in wild-type *Arabidopsis thaliana* cv. Columbia resulted in enhanced resistance to both salt and drought stresses (Hou et al., 2013).

TRIDC2AG073520 (TRITD2Av1G27893 in Svevo) is a G-type lectin S-receptor-like serine/threonine-protein kinase gene. The domesticated allele contains a nonsynonymous mutation expressed as an amino acid shift (isoleucine to threonine). This CG was significantly up-regulated under WL in IL20-2 (FC 2.29, P_{adj}=0.03). In *Arabidopsis*, drought and salinity stresses induced up-regulation of the gene (Sun et al., 2013). Moreover, the gene expressed specifically in root tissue, from early seedling stage to 50% of ear emergence (Supplemental Fig. S11;(Ramírez-González et al., 2018). Genetic dissection showed that the genomic region of this gene overlaps with a QTL affecting lateral root number per primary root (Maccaferri et al., 2016).

Two splice variance of TRITD2Av1G278930 were identified in the wild emmer genome (TRIDC2AG073520.1 and TRIDC2AG073520.2) included several mutations in each variant. The TRIDC2AG073520.1 variant is similar to the domesticated variant, although it contains a nonsynonymous SNP. The TRIDC2AG073520.2 variant is different in length and exon number; however, the domains remain similar to the domesticated variant and the extra exon is not characterized with a specific domain (Fig. 5C). The underline mechanisms by which the identified splice variance and/or amino acid substitution affect wild emmer response to stress via longer root systems is yet to be discovered.

Concluding remarks and future perspective

The current study targeted "lost alleles" from wild progenitor of wheat to understand their contribution to water stress response mechanisms. *In-depth* physiological characterization, high-throughput phonemics and functional genetics approaches revealed unique spatio-temporal water stress responsiveness dynamics strategies. Further characterization should emphasize the key role for modification of root-to-shoot ratio in response to stress as an adaptive trait. Our results suggest that re-introducing the wild genetic repertoire can enable

bioRxiv preprint doi: https://doi.org/10.1101/2020.06.17.157461; this version posted June 18, 2020. The copyright holder for this preprint (which was not certified by peer review) is the author/funder, who has granted bioRxiv a license to display the preprint in perpetuity. It is made available under aCC-BY-NC-ND 4.0 International license.

greater phenotypic plasticity and promote better resilience to anticipated unpredictable climatic conditions.

MATERIAL AND METHODES

Plant material and experimental design

Uniform seeds of 47 wild emmer wheat (*acc*. Zavitan) introgression lines (IL) in the background of elite durum wheat (*cv*. Svevo) and their recurrent parent were used for the current study. Detailed information for the ILs panel is provided in Supplementary Table S1. Seeds were surface disinfected (1% sodium hypochloric acid for 30 minutes) and placed in petri dishes on moist germination paper (Anchor Paper Co., St. Paul, MN, USA) about 3 cm apart, at 24ºC in the dark for 5 days. Three uniform seedlings from each line were transplanted to a single pot (2L, 45×19.5cm) filled with 1.2 kg of Fafard germination soil (Sungro, Massachusetts, USA), with osmocote fertilizer and Micromax micronutrients. Six days after transplanting (DAT), plants were thinned to one plant per pot. Pots were placed on automated carriers in the greenhouse (22/16°C day/night) and watered daily to 80% field capacity until the beginning of the experiment (11 DAT). The growth stages were tracked until the tillering stage (Zadoks stage 24-29; Zadoks et al., 1974). Water stress was initiated from the first day of imaging and the WL treatment pots reached the target field capacity within 16-24 days with average of 19 days after initiation of imaging. The daytime Photosynthetic Active Radiation (PAR) was supplemented with LED red/blue light lamps, with intensity of 200 μmol m^{-2} s^{-1}. The experiment was conducted at the Nebraska Innovation Campus greenhouse, high-throughput plant phenotyping core facilities (Scanalyzer 3D, LemnaTec Gmbh, Aachen, Germany), University of Nebraska-Lincoln.

A two-way factorial complete randomized experimental design, with 47 ILs and the recurrent parent, Svevo, was conducted. There were two irrigation treatments: well-watered (control, WW) at 80% field capacity (FC) and water-limited (WL) at 30% FC (Supplementary Fig. 12S), with three replicates for each combination. As quality control we used empty pots, placed randomly in every second row. In total there were 296 pots. Plants were imaged daily for 35 days with visible Red, Green and Blue (RGB) camera (Basler, Ahrensburg, Germany) taking 5 side-views (rotating 72°) and a single top-view. Image size was 2454×2056 pixels. After imaging, each pot was automatically weighed and watered to meet its calculated target weight. Greenhouse temperature kept at 22/16°C (day/night) during the experiment.

Based on results of the first experiment, we selected two ILs (IL20-2, IL46-3) for detailed

bioRxiv preprint doi: https://doi.org/10.1101/2020.06.17.157461; this version posted June 18, 2020. The copyright holder for this preprint (which was not certified by peer review) is the author/funder, who has granted bioRxiv a license to display the preprint in perpetuity. It is made available under aCC-BY-NC-ND 4.0 International license.

494 physiological characterization, alongside their parental line Svevo. A two-way factorial
495 complete random design was conducted, with three genotypes, and two irrigation treatments as
496 described above, with four replicates for a total 24 pots. The imaging started 7 DAT and
497 imaging continued for 14 days.
498
499 **Image processing**
500 PhenoImage GUI software (https://bit.ly/2OQzJoQ) was used for image processing based on
501 MATLAB (The Mathworks, Inc., Massachusetts, USA). Workflow consisted of three main
502 steps: image cropping, plant segmentation and attribute extraction. In brief, image cropping was
503 used to remove the frame of the chamber, followed by a background removal step based on
504 color differences. Plant segmentation was based on filtration of pixel intensity (i.e.,
505 distinguishing between plant and non-plant pixels). As a result, the software can give the plant
506 dimension, pixel sum, image moment and convex area.
507
508 **Morpho-physiological trait characterization**
509 *Plant height* and *plant width* were calculated from plant dimensions. *Plant architecture* (convex
510 area) was calculated to predict plant architecture trajectory. *Density* was calculated based on
511 the ratio between pixel sum and plant architecture. *Plant biomass* was calculated based on
512 projected shoot area (PSA) as described by (Campbell et al., 2015). On the last day of the
513 experiment, a subset of 19 ILs were harvested, oven dried (80^{o}C) and weighed to obtain shoot
514 dry weight. Correlation analysis showed high correlation between PSA and shoot dry weight
515 (r=0.96; $P<10^{-4}$; Supplementary Fig. S13). *Relative growth rate* (RGR) was calculated by
516 dividing daily pixel accumulation with pixel number from the previous day. Daily *water-use*
517 *efficiency* (WUE_t) was calculated as described by Momen et al. (2019), were (t) represents the
518 day.

519 $$\mathrm{WUE}_t = \frac{\Delta PSA\ (Pixels)}{\Delta \mathrm{WU}\ (ml)}$$

520 where ΔPSA is the daily PSA:

521 $$\Delta PSA = \mathrm{PSA}_{t-1} - \mathrm{PSA}_t$$

522 and ΔWU is the daily water used:

523 $$\Delta \mathrm{WU} = \mathrm{Pot\ weight}_{t-1} - \mathrm{Pot\ weight}_t$$

524
525 *Photosynthetic rate, transpiration rate* and *stomatal conductance* were measured between 10
526 and 22 DAT using a portable infra-red gas analyzer (LI-6800XT; Li-Cor Inc., Lincoln, NE,

bioRxiv preprint doi: https://doi.org/10.1101/2020.06.17.157461; this version posted June 18, 2020. The copyright holder for this preprint (which was not certified by peer review) is the author/funder, who has granted bioRxiv a license to display the preprint in perpetuity. It is made available under aCC-BY-NC-ND 4.0 International license.

USA). Measurements were conducted at the mid portion of the last fully expended leaf from 9:00 to 13:00 (n=3).

Root biomass was measured at 22 DAT. Root tissue was harvested (n=4), washed and oven dried (80^{o}C) for 72h, and weighed to obtain root dry weight. *Root-to-shoot ratio* was calculated by dividing root dry weight with PSA (shoot biomass).

Characterization of root and shoot length

Uniform seeds were germinated in a petri dish on moist germination paper for 5d in the dark at 22-25°C. Five seedlings of each genotype were placed on moist germination paper (25 × 38 cm; Anchor Paper Co., St. Paul, MN, USA), about 5 cm apart, with the germ end facing down. The paper was covered with another sheet of moist germination paper and rolled to a final diameter of 3 cm. The bases of the rolls were placed on a 4L beaker in a darkened growth chamber at a temperature of 24C/16C, 15h/9h day/night, at 50-60% relative humidity. Two-way factorial design was used with two genotypes (IL20-2 and Svevo) and two water availabilities: WW and WL, with 8 replicates for each combination (total of 32). Eight cigar rolls were placed in a container (4 L) with 100 ml (daily) for WW, or 20 ml (without refilling) for WL. Each container was wrapped with plastic to prevent water evaporation. Shoot and root length where measured daily by scale, from 3 to 8 DAT.

Statistical Analyses

The JMP® ver. 14 statistical package (SAS Institute, Cary, NC, USA) was used for statistical analyses, unless otherwise specified. Longitudinal response was fitted for genotypes (collectively or separately) under each water treatment. Analysis of Variance (ANOVA) was used to assess the possible effects of genotype (G), environment (E), and G×E interactions on morpho-physiological traits of genotypes. Frequency distribution was determined for all morpho-physiological traits on the last day. Principle Component Analysis (PCA) was used to determine associations between traits. PCA was based on a correlation matrix and is presented as biplot ordinations of the ILs (PC scores). Three components were extracted using eigenvalues >1.2 to ensure meaningful implementation of the data by each factor. An agglomerative hierarchical procedure with an incremental sum of squares grouping strategy, was employed using the Ward's method (Ward 1963), for the purpose of classification. Pearson correlation for all morpho-physiological traits was conducted for each water treatment. Drought-susceptibility index (S) was calculated according to Fischer and Maurer (1978):

bioRxiv preprint doi: https://doi.org/10.1101/2020.06.17.157461; this version posted June 18, 2020. The copyright holder for this preprint (which was not certified by peer review) is the author/funder, who has granted bioRxiv a license to display the preprint in perpetuity. It is made available under aCC-BY-NC-ND 4.0 International license.

$$S = \frac{1 - Y_{WL}/Y_{WW}}{1 - X_{WL}/X_{WW}}$$

where Y_{WL} and Y_{WW} are the mean phenotypic values of a certain genotype under the respective treatments, and X_{WL} and X_{WW} are the mean performances of all genotypes.

Morpho-physiological correlation matrix and Density distribution were plotted with R software (RStudio Team, 2015).

Broad-sense heritability dynamics

Broad-sense heritability ($_{bs}h^2$) and its components, genetic component (σ_g^2), and G×E interaction ($\sigma_{g\times e}^2$), were calculated for each day of imaging across the two water treatments using ANOVA-based variance components:

$$h^2 = \sigma_g^2/\sigma_g^2 + \sigma_{g\times e}^2/e,$$

where $\sigma_g^2 = [(MS_{IL} - MS_{IL\times e})/e]$, $\sigma_{g\times e}^2 = MS_{IL\times e}$, e is the number of water treatments and MS is the mean square.

RNA extraction and sequencing

Root tissues were collected daily (8-11 day after germination) and frozen in liquid nitrogen until RNA extraction. RNA was extracted using the plant/fungi total RNA purification kit (Norgen Biotek Corp., Canada) with on-column DNase treatment (Qiagen, Germany). Sample contamination and RNA integrity were assessed using ND-1000 spectrophotometer (Thermo Fisher Scientific). Based on the physiological analysis, we selected samples from day six for RNAseq, with two repeats for each combination (total 8). Single end (150bp) bar-coded cDNA libraries were prepared for sequencing on the Illumina HiSeq2000 sequencer (NGS Core, Nebraska Medical Center Omaha, USA).

Data processing and analysis

FastQ quality of each sample was manually inspected using FastQC (http://www.bioinformatics.babraham.ac.uk/projects/fastqc). Barcode removal, filtering and trimming of low-quality reads were executed using the command line tools Trimmomatic (Bolger et al., 2014). Each RNA-seq read was trimmed to make sure the average quality score exceeded 30 and has a minimum length of 70bp. Sequences were aligned to the available Svevo and Zavitan reference genomes using TopHat (Trapnell et al., 2009), allowing for up to 2 bp

bioRxiv preprint doi: https://doi.org/10.1101/2020.06.17.157461; this version posted June 18, 2020. The copyright holder for this preprint (which was not certified by peer review) is the author/funder, who has granted bioRxiv a license to display the preprint in perpetuity. It is made available under aCC-BY-NC-ND 4.0 International license.

mismatches per read. Reads mapped to multiple genomic locations were removed. Numbers of reads per gene were counted by the software tool of HTSeq-count using corresponding rice gene annotations and the "union" resolution mode was used (http://www-huber.embl.de/users/anders/HTSeq/). Differential expression analysis of count data and data visualization were conducted with the DESeq2 package (Love et al., 2014). To detect significant DEGs, a 5% false discovery rate (FDR) correction for multiple comparisons was determined (Benjamini and Hochberg, 1995), and a minimal |0.5| $\log_2$FC threshold was applied. Venn diagrams were created with http://bioinformatics.psb.ugent.be/webtools/Venn. Gene ontology, Singular Enrichment Analysis (SEA) and Parametric Analysis of DEGs set Enrichment for biological processes and pathways was conducted with AgriGO (http://systemsbiology.cau.edu.cn/agriGOv2; Tian et al., 2017).

Gene ontology network

Biological processes and molecular function networks were established using the DEGs GO terms with REVIGO software (http://revigo.irb.hr); this summarizes lists of GO terms using a clustering algorithm that relies on semantic similarity measures (Supek et al., 2011). The analysis outputs were transferred to the Cytoscape software (https://cytoscape.org/), which served as a network biology analysis and visualization tool (Otasek et al., 2019).

Genetic analysis of candidate DEGs

Candidate genes were analyzed on the wheat efp browser for expression in different tissues and phenological stages (http://bar.utoronto.ca/efp_wheat/cgi-bin/efpWeb.cgi; Ramírez-González et al., 2018). Gene sequences were compared with the publically available genome of Svevo https://wheat.pw.usda.gov/GG3/genome_browser and compared to Zavitan gene sequences with blast against the Zavitan genome https://wheat.pw.usda.gov/cgi-bin/seqserve/blast_wheat.cgi. Differences in splice variance number of candidate genes were perceived from blast on the GrainGenes website https://wheat.pw.usda.gov/cgi-bin/seqserve/blast_wheat.cgi. DNA translation to amino acids was done with the free online software https://web.expasy.org/translate

bioRxiv preprint doi: https://doi.org/10.1101/2020.06.17.157461; this version posted June 18, 2020. The copyright holder for this preprint (which was not certified by peer review) is the author/funder, who has granted bioRxiv a license to display the preprint in perpetuity. It is made available under aCC-BY-NC-ND 4.0 International license.

Supplemental Data

The following supplemental materials are available.

Supplemental Table S1. List of ILs and their chromosomal introgressions.

Supplemental Table S2. Correlations between morpho-physiological traits under well-watered and water-limited treatments.

Supplemental Table S3. Longitudinal coefficient of variance for PSA.

Supplemental Table S4. Comparison of morpho-physiological under two water treatments throughout the experiment for each cluster.

Supplemental Table S5. Regression equation of relative growth rate.

Supplemental Table S6. Comparisons of A, T and *gsw* between Svevo, IL20-2 and IL46-3 under two irrigation regimes throughout the experiment.

Supplemental Table S7. Comparisons of morpho-physiological traits between Svevo, IL20-2 and IL46-3 under two irrigation regimes.

Supplemental Table S8. Gene annotation within IL20-2 introgressions.

Supplemental Table S9. Hybrid genome significant differentially expressed genes.

Supplemental Table S10. Root-related candidate genes.

Supplemental Figure S1. Frequency distribution of continuance morpho-physiological traits under two irrigation regimes.

Supplemental Figure S2. Correlation matrix between morpho-physiological traits under (**A**) well-watered and (**B**) water-limited treatments.

Supplemental Figure S3. Principal component analysis of morpho-physiological traits.

Supplemental Figure S4. (**A**) Hierarchal clustering of morpho-physiological traits under WL and in terms of S index. (**B**) Clusters expression pattern.

Supplemental Figure S5. Longitudinal responsiveness dynamic of plant architecture and density.

Supplemental Figure S6. Longitudinal heritability of plant density and architecture.

Supplemental Figure S7. Longitudinal dynamics of transpiration rate.

Supplemental Figure S8. Longitudinal dynamics of shoot, root, root-to-shoot under contrasting water treatment.

Supplemental Figure S9. Differentially expressed gene ontology of (**A**) biological processes and (**B**) molecular function.

Supplemental Figure S10. Heat map of candidate genes from Zavitan expression atlas.

Supplemental Figure S11. Expression atlas of TRIDC2AG073520 in the wheat efp browser.

Supplemental Figure S12. Experimental design.

bioRxiv preprint doi: https://doi.org/10.1101/2020.06.17.157461; this version posted June 18, 2020. The copyright holder for this preprint (which was not certified by peer review) is the author/funder, who has granted bioRxiv a license to display the preprint in perpetuity. It is made available under aCC-BY-NC-ND 4.0 International license.

655 **Supplemental Figure S13.** Correlation between projected shoot area (PSA) and biomass DW.

656

657

658 ## Acknowledgments

659 We thank members of the Peleg and Walia labs for technical assistance with experiments. This
660 research was partially supported by the Chief Scientist of the Israel Ministry of Agriculture and
661 Rural Development to ZP, the U.S. Agency for International Development Middle East
662 Research and Cooperation (grant # M34-037) to ZP and the Agricultural Research Division
663 Wheat Innovation Fund from University of Nebraska-Lincoln to HW and TA.

664

bioRxiv preprint doi: https://doi.org/10.1101/2020.06.17.157461; this version posted June 18, 2020. The copyright holder for this preprint (which was not certified by peer review) is the author/funder, who has granted bioRxiv a license to display the preprint in perpetuity. It is made available under aCC-BY-NC-ND 4.0 International license.

LITERATURE CITED

Akpinar BA, Kantar M, Budak H (2015) Root precursors of microRNAs in wild emmer and modern wheats show major differences in response to drought stress. Funct Integr Genomics **15**: 587–598

Appels R, Eversole K, Feuillet C, Keller B, Rogers J, Stein N, Pozniak CJ, Choulet F, Distelfeld A, Poland J, et al. (2018) Shifting the limits in wheat research and breeding using a fully annotated reference genome. Science **361**: eaar7191

Araus JL, Slafer GA, Reynolds MP, Royo C (2002) Plant breeding and drought in C_3 cereals: What should we breed for? Ann Bot **89**: 925–940

Arms EM, Bloom AJ, St. Clair DA (2015) High-resolution mapping of a major effect QTL from wild tomato Solanum habrochaites that influences water relations under root chilling. Theor Appl Genet **128**: 1713–1724

Avni R, Nave M, Barad O, Baruch K, Twardziok SO, Gundlach H, Hale I, Mascher M, Spannagl M, Wiebe K, et al. (2017) Wild emmer genome architecture and diversity elucidate wheat evolution and domestication. Science **357**: 93–97

Baum M, Grando S, Backes G, Jahoor A, Sabbagh A, Ceccarelli S (2003) QTLs for agronomic traits in the Mediterranean environment identified in recombinant inbred lines of the cross "Arta" x *H. spontaneum* 41-1. Theor Appl Genet **107**: 1215–1225

Benjamini Y, Hochberg Y (1995) Controlling the false discovery rate: A practical and powerful approach to multiple testing. J R Stat Soc B **57**: 289–300

Blum A (1988) Plant breeding for stress environments. CRC Press

Bohnert HJ, Sheveleva E (1998) Plant stress adaptations--making metabolism move. Curr Opin Plant Biol **1**: 267–274

Bolger AM, Lohse M, Usadel B (2014) Trimmomatic: A flexible trimmer for Illumina sequence data. Bioinformatics **30**: 2114-2120.

Bradshaw AD (1965) Evolutionary significance of phenotypic plasticity in plants. Adv Genet **13**: 115-155

Brouns F, van Rooy G, Shewry P, Rustgi S, Jonkers, D (2019) Adverse reactions to wheat or wheat components. Compr Rev Food Sci Food Saf **18**: 1437-1452

Campbell MT, Knecht AC, Berger B, Brien CJ, Wang D, Walia H (2015) Integrating image-based phenomics and association analysis to dissect the genetic architecture of temporal salinity responses in rice. Plant Physiol **168**: 1476–1489

Chaves MM, Flexas J, Pinheiro C (2009) Photosynthesis under drought and salt stress: Regulation mechanisms from whole plant to cell. Ann Bot **103**: 551–560

bioRxiv preprint doi: https://doi.org/10.1101/2020.06.17.157461; this version posted June 18, 2020. The copyright holder for this preprint (which was not certified by peer review) is the author/funder, who has granted bioRxiv a license to display the preprint in perpetuity. It is made available under aCC-BY-NC-ND 4.0 International license.

Fischer RA, Maurer R (1978) Drought resistance in spring wheat cultivars. I. Grain yield responses. Aust J Agric Res **29**: 897–912

Gioia T, Nagel KA, Beleggia R, Fragasso M, Ficco DBM, Pieruschka R, De Vita P, Fiorani F, Papa R (2015) Impact of domestication on the phenotypic architecture of durum wheat under contrasting nitrogen fertilization. J Exp Bot **66**: 5519–5530

Golan G, Ayalon I, Perry A, Zimran G, Ade-Ajayi T, Mosquna A, Distelfeld A, Peleg Z (2019) *GNI-A1* mediates trade-off between grain number and grain weight in tetraploid wheat. Theor Appl Genet **132**: 2353–2365

Golan G, Hendel E, Méndez Espitia GE, Schwartz N, Peleg Z (2018) Activation of seminal root primordia during wheat domestication reveals underlying mechanisms of plant resilience. Plant Cell Environ **41**: 755–766

Gupta A, Rico-Medina A, Caño-Delgado AI (2020) The physiology of plant responses to drought. Science **368**: 266-269

Hou X, Liang Y, He X, Shen Y, Huang Z (2013) A novel ABA-responsive *TaSRHP* gene from wheat contributes to enhanced resistance to salt stress in *Arabidopsis thaliana*. Plant Mol Biol Report **31**: 791–801

Colette A, Bochdanovits Z, Jansweijer VMA, Koning FG, Berke L, Sanchez-Perez GF, Scheres B, Heidstra R (2011) Probing the roles of LRR RLK genes in *Arabidopsis thaliana* roots using a custom T-DNA insertion set. Plant Mol Biol **76**: 69–83

Kissoudis C, van de Wiel C, Visser RGF, van der Linden G (2016) Future-proof crops: challenges and strategies for climate resilience improvement. Curr Opin Plant Biol **30**: 47–56

Knecht AC, Campbell MT, Caprez A, Swanson DR, Walia H (2016) Image Harvest: An open-source platform for high-throughput plant image processing and analysis. J Exp Bot **67**: 3587–3599

Kooyers NJ (2015) The evolution of drought escape and avoidance in natural herbaceous populations. Plant Sci **234**: 155–162

Laurie S, Halford NG (2001) The role of protein kinases in the regulation of plant growth and development. Plant Growth Regul **34**: 253–265

Lopes MS, El-Basyoni I, Baenziger PS, Singh S, Royo C, Ozbek K, Aktas H, Ozer E, Ozdemir F, Manickavelu A, et al (2015) Exploiting genetic diversity from landraces in wheat breeding for adaptation to climate change. J Exp Bot **66**: 3477–3486

Love MI, Huber W, Anders S (2014) Moderated estimation of fold change and dispersion for RNA-seq data with DESeq2. Genome Biol **15**: 550

bioRxiv preprint doi: https://doi.org/10.1101/2020.06.17.157461; this version posted June 18, 2020. The copyright holder for this preprint (which was not certified by peer review) is the author/funder, who has granted bioRxiv a license to display the preprint in perpetuity. It is made available under aCC-BY-NC-ND 4.0 International license.

Maccaferri M, El-Feki W, Nazemi G, Salvi S, Canè MA, Colalongo MC, Stefanelli S, Tuberosa R (2016) Prioritizing quantitative trait loci for root system architecture in tetraploid wheat. J Exp Bot **67**: 1161–1178

Maccaferri M, Harris NS, Twardziok SO, Pasam RK, Gundlach H, Spannagl M, Ormanbekova D, Lux T, Prade VM, Milner SG, et al. (2019) Durum wheat genome highlights past domestication signatures and future improvement targets. Nat Genet **51**: 885–895

Merchuk-Ovnat L, Fahima T, Ephrath JE, Krugman T, Saranga Y (2017) Ancestral QTL alleles from wild emmer wheat enhance root development under drought in modern wheat. Front Plant Sci **8**: 1–12

Momen M, Campbell MT, Walia H, Morota G (2019) Utilizing trait networks and structural equation models as tools to interpret multi-trait genome-wide association studies. Plant Methods **15**:107

Myers SS, Smith MR, Guth S, Golden CD, Vaitla B, Mueller ND, Dangour AD, Huybers P (2017) Climate change and global food systems: Potential impacts on food security and undernutrition. Annu Rev Public Health **38**: 259–277

Nietzsche M, Landgraf R, Tohge T, Börnke F (2016) A protein-protein interaction network linking the energy-sensor kinase SnRK1 to multiple signaling pathways in *Arabidopsis thaliana*. Curr Plant Biol **5**: 36–44

Opanowicz M, Vain P, Draper J, Parker D, Doonan JH (2008) *Brachypodium distachyon*: making hay with a wild grass. Trends Plant Sci **13**: 172–177

Otasek D, Morris JH, Bouças J, Pico AR, Demchak B (2019) Cytoscape automation: Empowering workflow-based network analysis. Genome Biol **20**: 1–15

Peleg Z, Fahima T, Abbo S, Krugman T, Nevo E, Yakir D, Saranga Y (2005) Genetic diversity for drought resistance in wild emmer wheat and its ecogeographical associations. Plant Cell Environ **28**: 176–191

Peleg Z, Saranga Y, Krugman T, Abbo S, Nevo E, Fahima T (2008) Allelic diversity associated with aridity gradient in wild emmer wheat populations. Plant Cell Environ **31**: 39–49

Placido DF, Campbell MT, Folsom JJ, Cui X, Kruger GR, Baenziger PS, Walia H (2013) Introgression of novel traits from a wild wheat relative improves drought adaptation in wheat. Plant Physiol **161**: 1806–1819

Poot P, Lambers H (2008) Shallow-soil endemics: Adaptive advantages and constraints of a specialized root-system morphology. New Phytol **178**: 371–381

bioRxiv preprint doi: https://doi.org/10.1101/2020.06.17.157461; this version posted June 18, 2020. The copyright holder for this preprint (which was not certified by peer review) is the author/funder, who has granted bioRxiv a license to display the preprint in perpetuity. It is made available under aCC-BY-NC-ND 4.0 International license.

Ramírez-González RH, Borrill P, Lang D, Harrington SA, Brinton J, Venturini L, Davey M, Jacobs J, Van Ex F, Pasha A, et al. (2018) The transcriptional landscape of polyploid wheat. Science **361**: eaar6089.

Rellán-Álvarez R, Lobet G, Dinneny JR (2016) Environmental control of root system biology. Annu Rev Plant Biol **67**: 619–642

Reynolds MP, Hobbs PR, Braun HJ (2007) Challenges to international wheat improvement. J Agric Sci **145**: 223–227

Robbins NE, Dinneny JR (2015) The divining root: Moisture-driven responses of roots at the micro- and macro-scale. J Exp Bot **66**: 2145–2154

Rodrigues M, Chaves M, Wendler R, David M, Quick W, Leegood R, Stitt M, Pereira J (1993) Osmotic adjustment in water stressed grapevine leaves in relation to carbon assimilation. Funct Plant Biol **20**: 309

Rojas M, Lambert F, Ramirez-Villegas J, Challinor AJ (2019) Emergence of robust precipitation changes across crop production areas in the 21st century. Proc Natl Acad Sci USA **116**: 6673–6678

Roucou A, Violle C, Fort F, Roumet P, Ecarnot M, Vile D (2018) Shifts in plant functional strategies over the course of wheat domestication. J Appl Ecol **55**: 25–37

RStudio Team (2015) RStudio: Integrated Development Environment for R.

Sherrard ME, Maherali H (2006) The adaptive significance of drought escape in *Avena barbata*, an annual grass. Evolution **60**: 2478-2489

Shipley B, Meziane D (2002) The balanced-growth hypothesis and the allometry of leaf and root biomass allocation. Funct Ecol **16**: 326–331

Siddique KHM, Tennant D, Perry MW, Belford RK (1990) Water use and water use efficiency of old and modern wheat cultivars in a Mediterranean-type environment. Aust J Agric Res **41**: 431–447

Sun XL, Yu QY, Tang LL, Ji W, Bai X, Cai H, Liu XF, Ding XD, Zhu YM (2013) GsSRK, a G-type lectin S-receptor-like serine/threonine protein kinase, is a positive regulator of plant tolerance to salt stress. J Plant Physiol **170**: 505–515

Supek F, Bošnjak M, Škunca N, Šmuc T (2011) Revigo summarizes and visualizes long lists of gene ontology terms. PLoS One **6**: e21800

Teotia S, Lamb RS (2011) RCD1 and SRO1 are necessary to maintain meristematic fate in *Arabidopsis thaliana*. J Exp Bot **62**: 1271–1284

Tian T, Liu Y, Yan H, You Q, Yi X, Du Z, Xu W, Su Z (2017) AgriGO v2.0: A GO analysis toolkit for the agricultural community. Nucleic Acids Res **45**: 122–129

bioRxiv preprint doi: https://doi.org/10.1101/2020.06.17.157461; this version posted June 18, 2020. The copyright holder for this preprint (which was not certified by peer review) is the author/funder, who has granted bioRxiv a license to display the preprint in perpetuity. It is made available under aCC-BY-NC-ND 4.0 International license.

Trapnell C, Pachter L, Salzberg SL (2009). TopHat: Discovering splice junctions with RNA-Seq. Bioinformatics. **25**: 1105–11.

Tsujimura Y, Sugiyama S, Otsuka K, Htun TM, Numaguchi K, Castillo C, Akagi T, Ishii T, Ishikawa R (2019) Detection of a novel locus involved in non-seed-shattering behaviour of Japonica rice cultivar, *Oryza sativa* 'Nipponbare'. Theor Appl Genet **132**: 2615–2623

Virlet N, Sabermanesh K, Sadeghi-Tehran P, Hawkesford MJ (2017) Field Scanalyzer: An automated robotic field phenotyping platform for detailed crop monitoring. Funct Plant Biol **44**: 143–153

Voss-Fels KP, Robinson H, Mudge SR, Richard C, Newman S, Wittkop B, Stahl A, Friedt W, Frisch M, Gabur I, et al. (2018) *VERNALIZATION1* modulates root system architecture in wheat and barley. Mol Plant **11**: 226–229

Ward Jr, Joe H (1963) Hierarchical grouping to optimize an objective function. Assoc Stat Am J **58**: 236-244

Yang W, Feng H, Zhang X, Zhang J, Doonan JH, Batchelor WD, Xiong L, Yan J (2020) Crop phenomics and high-throughput phenotyping: Past decades, current challenges, and future perspectives. Mol Plant **13**: 187–214

Yang Z, Zheng H, Wei X, Song J, Wang B, Sui N (2018) Transcriptome analysis of sweet Sorghum inbred lines differing in salt tolerance provides novel insights into salt exclusion by roots. Plant Soil **430**: 423–439

Zadoks JC, Chang TT, Konzak CF, Fryer JD (1974) A decimal code for the growth stages of cereals. Weed Res **14**: 415-421